Characterization of a new magnesium hydrogen orthophosphate salt, $Mg_{3.5}H_2(PO_4)_3$, synthesized in supercritical water

Hassane Assaaoudi [a,b], Zhen Fang [b], Ian S. Butler [a,*], Dominic H. Ryan [c],
Janusz A. Kozinski [b]

[a] Department of Chemistry, Otto Maass Building, McGill University, 801 Sherbrooke Street West, Montreal, Quebec H3A 2K6, Canada
[b] Energy and Environmental Research Group, Department of Mining, Metals and Materials Engineering, Wong Building, Room 2290,
McGill University, 3610 University Street, Montreal, Quebec H3A 2B2, Canada
[c] Department of Physics and Centre for the Physics of Materials, 3600 University Street, McGill University, Montreal, Quebec H3A 2T8, Canada

Abstract

Beige crystals of a new magnesium hydrogen orthophosphate salt, $Mg_{3.5}H_2(PO_4)_3$, as well as nanoparticles of an amorphous, non-Mg-containing phosphate material, $Fe_{1-y}K_yPO_4$ ($0 < y < 1$), have been produced by hydrothermal reactions in supercritical water (SCW) of equivalent quantities of aqueous $MgCl_2 \cdot 6H_2O$ (2 M), and $K_4P_2O_7$ (1 M) in concentrated HCl in a stainless-steel batch reactor at 400–450 °C and 25–32 MPa. The new salt has been characterized by single-crystal X-ray diffraction and IR and Raman spectroscopies. It crystallizes in the triclinic space group $P\bar{1}$, $Z = 2$ with the following unit-cell parameters: $a = 6.438(1)$, $b = 7.856(1)$, $c = 9.438(1)$ Å; $\alpha = 104.57(1)$, $\beta = 108.61(1)$, $\gamma = 101.28(1)°$, $V = 739.99$ Å^3. The effects of the SCW conditions on the nature of the products and their yields and morphologies have been studied by IR and Raman spectroscopies, X-ray powder diffraction, X-ray energy dispersive analysis, scanning electron microscopy, transmission electron microscopy and inductively coupled plasma analysis.
© 2007 Elsevier Masson SAS. All rights reserved.

Keywords: Supercritical water; IR and Raman spectra; Magnesium; Orthophosphate; Nanomaterial

1. Introduction

Inorganic phosphates encompass a large class of diverse materials with numerous important industrial uses, e.g., as catalysts, ion-exchange materials, solid electrolytes for batteries, in linear and non-linear optical components, as chelating agents, in synthetic replacements for bone and teeth, and as phosphors, detergents and fertilizers [1,2]. Inorganic phosphates may, in fact, represent perhaps one of the most interesting types of new inorganic materials, in large part, due to the ability of the tetrahedral PO_4^{3-} group to bond with other structural units.

Our decision to work on magnesium hydrogen phosphates, such as *newberyite* ($MgHPO_4 \cdot 3H_2O$), and its anhydrous form, $MgHPO_4$, was indeed motivated by the interesting range of applications known for these particular phosphate materials, *newberyite* occurs naturally in bat and bird guano, as well as in both human and animal urinary stones [3,4]. Prior to the development of life on the Earth, *newberyite*, may have preceded organogenic apatite as the dominant inorganic phosphate mineral being formed in the primordial ocean. *Newberyite*, together with another phosphate mineral, *brushite* ($CaHPO_4 \cdot 2H_2O$), may have contributed to pre-enzymatic phosphorylation and thus to the development of life itself [5]. Furthermore, the growth of single-crystals of anhydrous magnesium hydrogen phosphate ($MgHPO_4$) is of considerable interest, especially in fundamental studies of phase transitions and because of their important dielectric, ferroelectric, piezoelectric and optical

* Corresponding author. Tel.: +1 514 398 6910.
E-mail address: ian.butler@mcgill.ca (I.S. Butler).

properties. The crystals are used in transducers and in many linear and non-linear mechanical devices, as well as being suitable for testing the microscopic theory of ferroelectricity [6].

A considerable body of data has been reported on the physico-mechanical properties of hardened cements containing magnesium phosphates as binders in which the hardening is a consequence of reactions between metal oxides and phosphates. The number of possible applications of this class of binders is steadily increasing [7]. Moreover, the presence of protons in such materials is very important, since protons often have properties markedly different from those of other monovalent cations [8]. A proton has the smallest mass, its mobility varies over ten orders of magnitude depending on its chemical bonding state in condensed phases, and its interactions with materials result in significant changes in chemical and physical properties. Modification of materials by chemical reactions with protons has been demonstrated in a wide variety of fields, e.g., the implantation of protons offers novel possibilities for studying electronic excitation effects and the creation of new materials. For instance, the effect of H^+ implantation on magnesium phosphate has already led to the production of fast proton-conducting (120 keV, 1×10^{18} cm^{-2}) glasses [9].

Both near-critical and supercritical water (SCW) have been used as reaction media for the synthesis of highly crystalline metal oxides [10–13]. In a previous study, we applied the SCW approach to the production of highly crystalline and amorphous micro- and nanosized particles of a new phosphate material, $KCo_3Fe(PO_4)_3$ [14]. There is enormous interest in such nanoporous structures because of their considerable industrial potential in heterogeneous catalysis, gas absorption and ion-exchange systems. Micro- and nanoporous catalysts often display high selectivity because the channel apertures sometimes permit only certain reactants access to the catalytically active interior of the material and also may allow only certain reaction products to leave [15,16].

In this present paper, we report analytical, structural and spectroscopic data for a new crystalline magnesium hydrogen phosphate salt, $Mg_{3.5}H_2(PO_4)_3$, and amorphous nanoparticles of a non-Mg-containing phosphate material produced under SCW conditions. The effects of temperature, pH, and reaction time on the morphology of the particles being produced have also been investigated by various analytical and spectroscopic techniques.

2. Experimental section

2.1. Synthesis

Crystals of $Mg_{3.5}H_2(PO_4)_3$, as well as nanoparticles of a solid $Fe_{1-y}K_yPO_4$ ($0 < y < 1$) material, were obtained from the reaction between equivalent amounts of aqueous $MgCl_2 \cdot 6H_2O$ (2 M), and $K_4P_2O_7$ (1 M) in a pre-determined volume of concentrated HCl (35%), [V(HCl):V(Mg) = 3:5, 7:10 or 4:5 in a stainless-steel batch reactor of volume = 6 mL; length = 105 mm, o.d. = 12.7 mm (1/2 inch)]. Both the temperature and pressure were measured with

a pressure transducer fitted with a J-type thermocouple (Dynisco E242). The pressure was also calculated by knowing the density of water [(weight of water added)/(volume of batch reactor) ≈ 1.6 g/mL], assuming that only water contributed to the pressure. Bassett et al. [17] have compared the pressure values obtained by such calculations with the P–T boundary of the α-β-transition in quartz and have shown that the pressure difference is less than 4% between the two methods. Approximately 1 mL of the final solution was loaded into the reactor which, after sealing and connecting to a data acquisition system, was submerged in a fluidized sand bath (Omega FSB-3) or placed into a tubular furnace. The reactor was heated at a rate of 3.5 °C/s to 400–450 °C and then held at this temperature for 5, 10, 30, 60 or 120 min. After each given time period, the reactor was quenched in cold water and the reaction mixture was emptied into a flask. The reactor was washed with water and the washings were added to the same flask. The solution in the flask was filtered through a membrane filter to yield a solid phase, which was dried at room temperature. Well-shaped, beige crystals were produced under the conditions reported in Table 1. The aqueous phase was left at room temperature for about 1–2 h, after which a green–yellow powder appeared, which was subsequently filtered and analyzed (Table 1).

The SCW reaction conditions described above are essentially the same as those reported earlier for the preparation of $KCo_3Fe(PO_4)_3$ [14], except that the pH was lower and the reaction time was shorter (30 min instead of 60 min).

2.2. Spectroscopic and crystallographic analyses

Crystalline $Mg_{3.5}H_2(PO_4)_3$ was characterized by scanning electron microscopy (SEM), X-ray energy dispersive analysis (EDX), IR and Raman spectroscopies, and single-crystal X-ray diffraction. The $Fe_{1-y}K_yPO_4$ ($0 < y < 1$) powder produced in the SCW experiments was examined by X-ray powder diffraction (XRD), ICP chemical analyses, scanning electron microscopy (SEM), transmission electron microscopy (TEM), Raman spectroscopy and magnetic susceptibility measurements. Details of these various analytical studies are given below.

A vertical-goniometer X-ray diffractometer (Philips model PW1710), equipped with a Cu Kα radiation source, was used for the powder diffraction measurements. The samples were scanned over a 5–60° range, using a 0.02° 2θ step-size and a 0.5 s/step measurement time. ICP chemical analyses were performed on a Thermo Jarrell-Ash Trace Scan Axial Torch Sequential ICP system. The morphology of the particles was investigated using field-emission SEM (Model JSM-840) and TEM (Model JEOL EM2011) instruments. Both the crystals and the powders were studied by EDX (Model EDAX).

Infrared spectra were recorded at ambient temperature on a Bomem MB100 FT-IR spectrometer, at 2 cm^{-1} resolution (50 scans), using the KBr pellet technique. The wave number accuracy is considered to be within ±1 cm^{-1} for sharp bands. Raman spectra were measured on a Renishaw 3000 Raman microscope (20X objective), using the 514.5-nm line of an

Table 1
Experimental conditions and results

Run	HCl	T (°C)	P (MPa)	Products					
				0 min	5 min	10 min	30 min	1 h	2 h
1	0.6	400	25	–	P	P	P	P	P
2	0.7	450	32	–	P	P	P	P	P
3	0.8	25	0.1	–	–	–	–	–	$KMgHP_2O_7 \cdot 2H_2O$[a]
4	0.8	400	25	–	P	P	C + P	C + P	C + P
5	0.8	450	32	–	P	P	C + P	C + P	C + P

P: powder.
C: crystals of $Mg_{3.5}H_2(PO_4)_3$.
[a] Ref. [24].

Ar$^+$-ion laser for excitation (5–100 mW laser power; 1 cm^{-1} spectral slit-width; 5 s exposure time; 10 accumulations). The band positions are considered to be accurate to at least ±1 cm^{-1}.

The single-crystal X-ray diffraction work was performed on a Bruker D8 Discover diffractometer. The structure was solved by direct methods using SHELXS97 [18] and was refined by a full-matrix, least-squares technique SHELXL97 [19]. The molecular drawings, obtained with ORTEP III [20], were manipulated using the WINGX system of programs [21]. After checking the final residuals R and R$_w$ [$I > 2\sigma(I_{obs})$] and taking anisotropic thermal parameters into account, analysis of the X-ray data established the chemical formula of the new compound as $Mg_{3.5}H_2(PO_4)_3$.

3. Results and discussion

3.1. Identification of materials

The XRD patterns of the powders formed under SCW conditions indicated that the materials were amorphous. Subsequent ICP and EDX analyses of the powders showed that the Fe, Mg, K and P contents were closely similar to those obtained for the amorphous powder produced using a Co(II) salt [14] instead of a Mg(II) salt. The morphology of the particles and the distribution of their sizes were established by SEM and TEM (Fig. 1). Crystalline $Mg_{3.5}H_2(PO_4)_3$ and the powders were analyzed by EDX and the data showed that their compositions were different (Fig. 2). Irrespective of the experimental SCW conditions employed, the powder obtained did not contain any Mg. The carbon peaks appearing in Fig. 2(a) and (b) are associated with the agent used to immobilize the particles for analysis. The powder nanoparticles are spherical or in the form of fibers, and the size of the spherical particles range from 20 to 500 nm (Fig. 1(e) and (f)).

The iron present in the amorphous powder $Fe_{1-y}K_yPO_4$ ($0 < y < 1$) was most likely leached from the stainless-steel (SS-316) walls of the reactor by concentrated HCl under the SCW conditions employed. The formation of the amorphous powder may result from decomposition of $K_4P_2O_7$ in the presence of the corrosion products generated from the stainless-steel walls under the strongly acidic SCW conditions employed.

Charge compensation between the Mg^{2+} cations and the PO_4^{3-} anions is achieved by the addition of two protons. The structural determination for the new salt did not lead to R indices of less than 7.8% (for all data), most probably because of slight Fe contamination, as indicated by EDX analysis, and the strong SCW conditions employed, which favored fissuring of the single-crystals and scratching of their surfaces (Fig. 3). The salt crystallizes in the triclinic system with space group $P\bar{1}$, $Z = 2$, with unit-cell parameters: $a = 6.438(1)$ Å, $b = 7.856(1)$ Å, $c = 9.438(1)$, $\alpha = 104.57(1)$, $\beta = 108.61(1)$, $\gamma = 101.28(1)$, $V = 739.99$ Å^3.

Crystalline $Mg_{3.5}H_2(PO_4)_3$ exhibits infinite chains of edge-sharing PO_4^{3-}, [MgO_6] and [MgO_5] units, which form small tunnels, as shown in the ORTEP diagram (Fig. 4). The diagonal distance of hexagonal tunnels, located along the c-axis, is estimated to 5.21 Å. Because the high value of R indices detailed structure was not presented.

3.2. Effect of reaction temperature

Two temperatures (400 °C and 450 °C) were investigated using the SCW conditions employed. By comparison, production of the related crystalline Co(II) phosphate salt, $KCo_3Fe(PO_4)_3$ [14], was much more difficult at either temperature, but especially at 400 °C. The particles produced with Mg(II) at 450 °C (with all other conditions being kept constant) had a slightly narrower size distribution than did those obtained at 400 °C [14]. Generally, when the temperature of the SCW reactions was increased, the particle sizes decreased.

3.3. Effect of pH

The effect of pH was investigated by adjusting the amount of concentrated HCl added. The reaction between equivalent quantities of aqueous $MgCl_2 \cdot 6H_2O$ (2 M), and $K_4P_2O_7$ (1 M) was limited by the amount of HCl which could be added in order to avoid instantaneous precipitation from solution and yet still permit synthesis of $Mg_{3.5}H_2(PO_4)_3$ crystals under the SCW conditions employed [V(HCl):V(Co) = 3:5, 7:10 and 4:5]. The powder particles obtained with V(HCl):V(Co) = 4:5 were spherical with sponge-like morphology, which favored coagulation of the particles. When V(HCl):V(Co) = 3:5, however, the particles were produced as layers of fibers with sponge-like morphology (Fig. 1(c) and (d)).
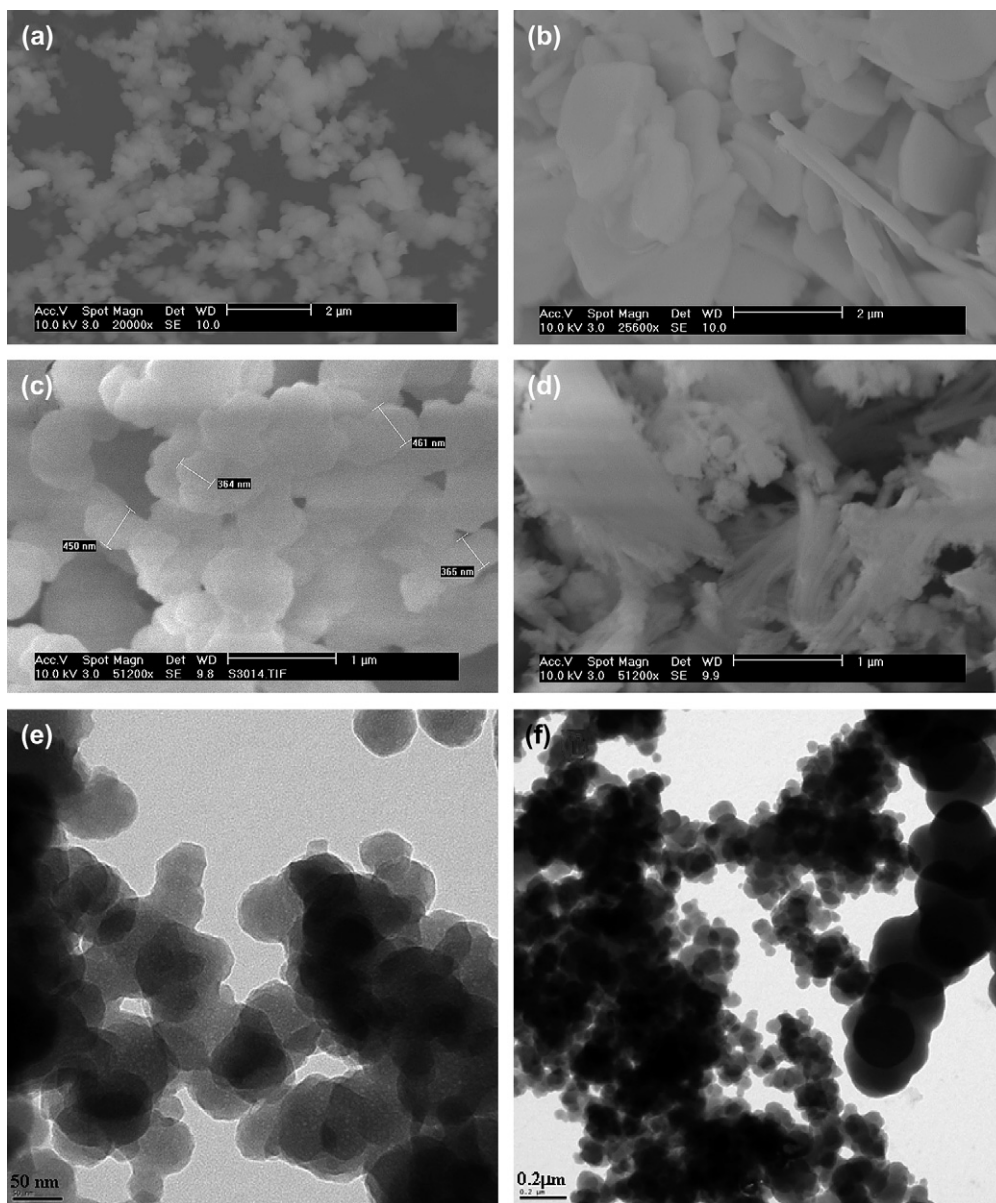
Fig. 1. Scanning electron microscope (SEM) (a, b, c, d) and transmission electronic microscopy TEM pictures (e, f) of amorphous powder obtained at 400 °C, 25 MPa, acidity $V(HCl):V(Mg) = 4:5$ and reaction time of (a) 30 min, (b) 120 min, showing the effect of reaction time on the morphology and particle size. The effect of pH is shown from SEM of amorphous powder obtained at 450 °C, 32 MPa, $\tau = 10$ min and pH, represented by ratio (c) $V(HCl):V(Mg) = 4:5$ and (d) $V(HCl):V(Mg) = 3:5$, (e, f) the size of spherical particles are from 20 to 500 nm.

3.4. Effect of residence time in the reactor

The influence of residence time in the reactor (τ) was investigated by performing the hydrothermal reactions at two different temperatures (400 °C and 450 °C), while keeping the $V(HCl):V(Co)$ ratio constant. For example, the effect of residence time on the production of crystalline $Mg_{3.5}H_2(PO_4)_3$ under the SCW conditions indicated as [450 °C, 32 MPa and $V(HCl):V(Co) = 4:5$] and reaction times $\tau = 5$, 10, 30, 60 and 120 min is shown in Fig. 5, while the morphologies of the particles produced are illustrated in Fig. 1(a) and 1(b). The particles exhibit distinct changes from spherical to layers with sponge-like morphology. The particles produced at

$\tau = 120$ min are lamellar, while those obtained after 30 min (Fig. 1(a)) have deformed spherical shapes.

In conclusion, therefore, depending on the pH of the reaction mixture, the particles can be produced in either spherical or fiber forms. When the residence time in the reactor is increased, the spheres become deformed and coagulate with layer morphology.

3.5. Vibrational spectra

Infrared and Raman spectroscopies play a prominent role in structural studies of inorganic materials, especially when X-ray diffraction methods fail to give unequivocal results, as

Fig. 2. EDX analysis of (a) crystalline $Mg_{3.5}H_2(PO_4)_3$ and (b) amorphous powder obtained after SCW reaction. The presence of Cd and Au is due to the coating procedure and the carbon comes from the type of carbon used to immobilize the samples.

in the case of glasses and amorphous substances. For this reason, harmonization of X-ray diffraction results with those from vibrational spectroscopy has become practically important. Recently, a linear empirical correlation was established [22] for crystalline inorganic phosphates between the wave numbers of the Raman-active P—O stretching modes and the associated P—O bond lengths. This correlation has been tested and extended with some success to glassy and amorphous phosphate materials, such as $Na_5Ti(PO_4)_3$ glass [23]. We have recently applied this correlation to the Raman spectra of $KCo_3Fe(PO_4)_3$ [14].

When the reaction mixture used for the production of crystalline $Mg_{3.5}H_2(PO_4)_3$ was allowed to stand at room temperature, $KMgHP_2O_7 \cdot 2H_2O$ was formed [24]. The IR spectra of the different products obtained under SCW conditions for reaction times $\tau = 0$ min (ambient conditions), 5 min, and between 5 and 120 min are shown in Fig. 6.

Fig. 3. Scanning electron microscopy pictures of crystal $Mg_{3.5}H_2(PO_4)_3$.

Fig. 4. ORTEP view of asymmetric unit with atomic numbering scheme of $Mg_{3.5}H_2(PO_4)_3$ (ellipsoids drawn at 50% probability level). Symmetry codes are indicated for each atom between parentheses.

3.5.1. $KMgHP_2O_7 \cdot 2H_2O$

The IR spectrum of $KMgHP_2O_7 \cdot 2H_2O$ is given in Fig. 6(a). Although this spectrum has been reported previously [24] it is worthwhile summarizing the results for the purposes of comparison with the spectra of the products formed in the present work.

The two broad IR bands located at around 3400 and 3280 cm^{-1} correspond to the OH stretching vibrations of the water molecules. The bending vibration of the water molecules is at 1685 cm^{-1} and the rocking band appears at 630 cm^{-1}. The symmetric stretching vibration of the H—O(P) bond is observed as a weak feature located at 2290 cm^{-1}, while the bending vibration is at 1447 cm^{-1}. The asymmetric and symmetric terminal stretching vibrations of PO_2 groups usually occur in the 1250—980 cm^{-1} region [25,26]. The intense band observed at 1218 cm^{-1} is attributed to the asymmetric terminal stretching vibration of the PO_2 group ($\nu_{as}PO_2$). The P—O(H) stretching mode is observed at 797 cm^{-1}, while the asymmetric POP bridge stretching vibration ($\nu_{as}POP$) occurs at 882 cm^{-1}. For the symmetric POP bridge vibrations (ν_sPOP), only one band is observed. The PO_2 rocking and the deformation modes are seen in the 600—400 cm^{-1} region [26].

Another interesting aspect of the vibrational spectra is the possibility of obtaining information about the configuration of the POP bridge from the data. The ν_sPOP vibrations are only observed in the Raman spectrum when the bridge is linear [25]. For the bent configuration, these vibrations appear in both the IR and Raman spectra. In our previous work on $KMgHP_2O_7 \cdot 2H_2O$ [24], the appearance of ν_sPOP at 698 and 709 cm^{-1} in the IR and Raman spectra, respectively, indicated a bent configuration of the P_2O_7 units. This conclusion is fully in agreement with the single-crystal X-ray diffraction results.

3.5.2. Sample obtained after 5 min under SCW conditions

The IR spectrum of the crystalline sample obtained from the reaction mixture after 5 min at 400 °C/25 MPa is shown in Fig. 6(b). On comparison with the IR data for $KMgHP_2O_7 \cdot 2H_2O$, there are several notable differences observed. First, there is an increase in the range of water

Fig. 5. Optical micrographs showing the evolution of products obtained from the reaction under SCW conditions [450 °C, 32 MPa and $V(HCl):V(Co) = 4:5$] after 5, 10, 30, 60 and 120 min.

frequencies, *viz.*, 3700–2700 *versus* 3400–3280 cm^{-1} for KMgHP$_2$O$_7$·2H$_2$O. This difference is due to changes in the nature of water bonding in the two materials. Secondly, the bending vibration of the water molecules is shifted from 1685 to 1640 cm^{-1}. This shift corresponds to a reduced force constant for the hydrogen-bonded water molecules in the two samples. Thirdly, the H$_2$O rocking mode, originally observed at 630 cm^{-1}, has disappeared. Fourthly, the symmetric stretching and bending H–O(P) vibrations have changed in frequency; the former is observed at 2380 cm^{-1}, while the latter is overlapped with the highest asymmetric stretching P–O band. Fifthly, the asymmetric POP bridge stretching vibration (ν_{as}POP) and the symmetric POP bridge vibrations (ν_sPOP), observed for KMgHP$_2$O$_7$·2H$_2$O, have disappeared. These observations indicate that the P$_2$O$_7^{4-}$ ions have been hydrolyzed to the more stable PO$_4^{3-}$ ions at high temperature and under pressure. This conclusion is in agreement with the numerous studies reported on the thermal stabilities of ortho- and pyrophosphates [27,28]. Finally, the deformation modes of the PO$_4^{3-}$ groups have merged into one large band located at 507 cm^{-1}, confirming the amorphous state of the sample. Moreover, the PO$_4^{3-}$ groups may be present in the form of the orthophosphate acids H$_2$PO$_4^-$ or HPO$_4^{2-}$ rather than as PO$_4^{3-}$, which have two different P–O(H) and P–O$_{ext}$ bond lengths and are characterized by bands at 1190 and 1080 cm^{-1} [29].

Recently, we have investigated the effects of pressure [30] and temperature [24] on KMgHP$_2$O$_7$·2H$_2$O. In the pressure study, the effects of high external pressures on the Raman spectra of KMgHP$_2$O$_7$·2H$_2$O and three related metal pyrophosphate dihydrates, KMHP$_2$O$_7$·2H$_2$O [M = Co(II), Mn(II), Zn(II)], were examined by diamond-anvil, cell Raman microspectroscopy for pressures up to ∼42 kbar. At ∼29 kbar, the ν_{as}POP band of the Co(II) compound disappears completely and irreversibly, suggesting the occurrence of a pressure-driven structural transformation or possibly even the initial stages of amorphization. No such dramatic spectral changes were observed for the Mg(II) pyrophosphate salt or for the other two metal pyrophosphates. In the temperature study, the structural changes occurring during thermal decomposition were monitored by TG–DSC, X-ray powder diffraction, and IR spectroscopy. When KMgHP$_2$O$_7$·2H$_2$O was heated gradually, it first became amorphous and then condensed to metaphosphate chains.

3.5.3. Mg$_{3.5}$H$_2$(PO$_4$)$_3$

The new orthophosphate salt, Mg$_{3.5}$H$_2$(PO$_4$)$_3$ crystallizes in the triclinic space group $P\bar{1}$ with $Z = 2$. The P atoms lie on C$_1$ sites. The IR and Raman spectra of the salt shown in Fig. 7, while the proposed vibrational assignments are given in Table 2. The presence of the bending vibrations H–O(P) at ∼1510 and
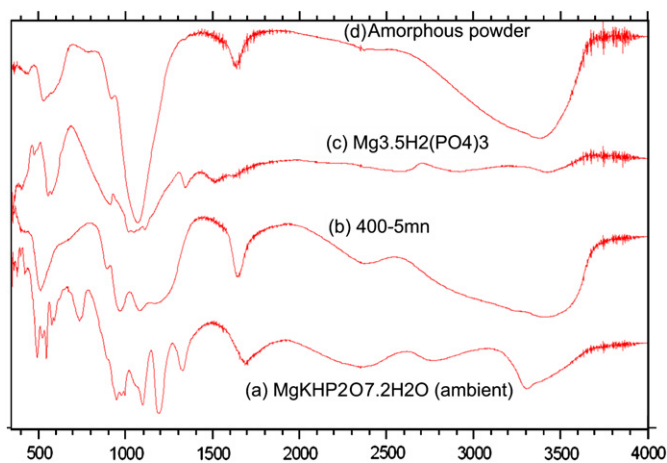
Fig. 6. Infrared spectra of different products obtained at (a) ambient conditions, which afforded crystals of MgKHP$_2$O$_7$·2H$_2$O; (b) 400 °C, 25 MPa, $\tau = 5$ min; (c) $T = 400$–450 °C, $P = 25$–32 MPa, $\tau \leq 30$ min; (d) $T = 400$–450 °C, $P = 25$–32 MPa, $5 < \tau \leq 120$ min.
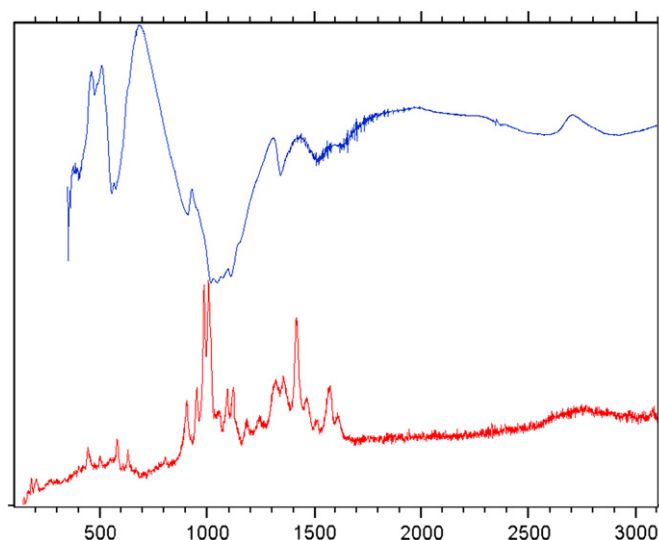
Fig. 7. Raman and infrared spectra of Mg$_{3.5}$H$_2$(PO$_4$)$_3$.

Table 2
Proposed IR band assignments (cm^{-1}) of the materials produced from the reactions of the Mg(II) salt under SCW conditions, compared to those obtained for KMgHP$_2$O$_7$·2H$_2$O at ambient conditions

Assignment pyrophosphate	KMgHP$_2$O$_7$·2H$_2$O (a)	Powder (b)	Mg$_{3.5}$H$_2$(PO$_4$)$_3$ (c)		Powder (d)	Assignment orthophosphate
			Ra	IR		
νH$_2$O	3400	3410	–	–	3475	νH$_2$O
	3280					
ν(HO)(−P)	2290	2380	–	–	–	ν(HO)(−P)
δH$_2$O	1685	1640	–	–	1635	δH$_2$O
δHO(−P)	1447	–	1600		–	δHO(−P)
			1570			
			1510	1510		
			1465			
			1419	1340		
			1350			
			1320			
			1245			
ν_{as}PO$_2$	1217	1190	1183	1145	1067	ν_{as}PO (ν_3)
ν_sPO$_2$	1187	1080	1120	1110		
ν_{as}P−OH	1118			1070		
	1100		1055	1050		
	1064		1012	1015		
	981					
		960	985	910	940	
			950			ν_sPO (ν_1)
		880	905		–	ν_{as}P−OH
ν_{as}POP	882	–	–	–	–	–
ν_sP−OH	797	–	803	–	–	ν_sP−OH
ν_sPOP	698	–	–	–	–	–
δPO$_2$ + ρPO$_2$ + ρH$_2$O			630			
	544		580	575		
				555	530	δ_{as}OPO (ν_4)
	500	503	500			
	437					
δPOP	377	420	440	475	440	δ_sOPO (ν_2)
	353					

The Raman data of the salt Mg$_{3.5}$H$_2$(PO$_4$)$_3$ are included.

1340 cm^{-1} confirms that the salt contains H atoms. The nature of the four normal vibrations [ν_1, ν_2, ν_3, and ν_4 in Herzberg notation [31]] of the PO$_4^{3-}$ groups was determined by the site group method of Halford [32], in which the normal modes of the free ion are correlated to the vibrations in the site and crystal (factor group) symmetry. Theoretically, each vibrational mode of the PO$_4^{3-}$ ions could be split into two components by dynamic coupling between the two equivalent anions in the primitive unit-cell. One component would be Raman-active, while the other would be IR-active. So, in this case, the effect of factor group does not result in an increase in the number of bands expected in the IR or in Raman. However, the factor group effect may be manifested by the non-coincidence between the IR and Raman spectra (Table 2). The full influence of the site and factor groups on the internal vibrations of the PO$_4^{3-}$ ions is, however,

not observed for each mode. For instance, the asymmetric P−O stretching vibration (ν_{as}PO or ν_3) and O−P−O bending vibration (ν_{as} O−P−O or ν_4) should be split into three IR and three Raman-active bands for each of the three different PO$_4^{3-}$ groups in crystalline Mg$_{3.5}$H$_2$(PO$_4$)$_3$, which would result in nine expected bands. However, only five bands are observed for ν_3 in both the IR and Raman spectra, while for ν_4, there are two IR and three Raman bands.

3.5.4. Sample obtained for more than 5 min reaction under SCW conditions

The IR spectra of the amorphous powders obtained under different SCW conditions for reaction times of at least 5 min at 450 °C and more than 5 min at 400 °C are identical and are represented by the spectrum shown in Fig. 6(d). This

spectrum indicates the presence of orthophosphate groups and, as expected for amorphous materials, the spectrum is characterized by broad bands and a relatively high and featureless background. In amorphous solids, dipole−dipole interactions between molecular vibrations are the most important source of inhomogeneous band broadening in the strongest IR absorption bands. The 1067 and 940 cm^{-1} bands correspond to asymmetric and symmetric P−O stretching modes, respectively, while the large band centered at 530 cm^{-1} and the weak one at 428 cm^{-1} are assigned to the asymmetric and symmetric O−P−O bending modes, respectively. The presence of the symmetric P−O stretching mode (ν_1) confirms that the symmetry of the anionic group PO_4^{3-} is not tetrahedral, even though the bands are close to the frequencies observed for the free anion PO_4^{3-}. The spectrum does not contain any bands related to H−O(P) or P−O(H), which can be attributed to the conversion of acid orthophosphate HPO_4^{2-} or $H_2PO_4^-$ to PO_4^{3-} anions under the strong SCW conditions employed.

3.5.5. Raman spectra of amorphous powder and the material produced by heating at 800 °C

The Raman spectra of the amorphous powder and the product obtained after heating at 800 °C are shown in Fig. 8. The X-ray powder diffraction pattern of the heated product exhibits high crystallinity, but it was not indexed. The Raman spectrum of the amorphous powder is the same as that for the amorphous material produced during the synthesis of KCo$_3$Fe(PO$_4$)$_3$ [14] and the spectra of the products obtained by heating at 800 °C are also closely similar.

4. Conclusions

Beige crystals of the new magnesium tri-orthophosphate salt, $Mg_{3.5}H_2(PO_4)_3$, as well as nanoparticles of an amorphous, non-Mg-containing material with an apparent composition $K_{0.56}Fe_{1.22}PO_4$, have been synthesized by hydrothermal reactions under SCW conditions. Depending on the pH of the reaction mixture, particles can be produced in either spherical or fiber forms. When the residence time in the reactor is increased, the spheres become deformed and coagulate with a layer morphology. In addition, the particle sizes decrease when the temperature of the SCW reactions is increased. The products have been characterized by various analytical techniques.
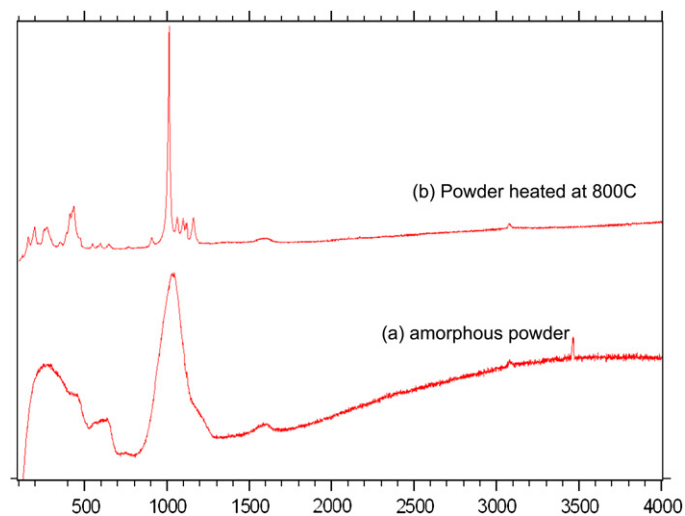
References

[1] G.R. Van Wazer, Phosphorus and its compounds, in: Chemistry, vol. 1, Interscience, New York, 1958.
[2] T. Kanazawa, Inorganic Phosphate Materials, Elsevier, New York, 1989.
[3] C. Hintze, Hanbuch der Mineralogie, vol. 1, De Grueyter, Berlin, 1933, (Part 4).
[4] D.J. Sutor, Newberyite, Nature 218 (1968) 295.
[5] B. Gedulin, G. Arrhenius, in: S. Bengston (Ed.), Early Life on Earth, Columbia University Press, May 1992 (Nobel Symposium 84).
[6] C.C. Desai, M. Shukla, J. Cryst. Res. Technol. 25 (8) (1990) 871−879.
[7] P. Marek, Mater. Res. Soc. Symp. Proc. 179 (1991) 83−86.
[8] F.M. Ernsberger, J. Am. Ceram. Soc. 66 (11) (1983) 747−750.
[9] H. Hosono, N. Ueda, H. Kawazoe, N. Matsunami, J. Non-Cryst. Solids 182 (1995) 109−118.
[10] A. Cabanas, J.A. Darr, M. Poliakoff, E. Lester, Chem. Commun. 11 (2000) 901−902.
[11] T. Adschiri, K. Kanazawa, K. Arai, J. Am. Ceram. Soc. 75 (9) (1992) 2615−2618.
[12] J.A. Darr, M. Poliakoff, Chem. Rev. 99 (1999) 495−542.
[13] A. Cabanas, M. Poliakoff, J. Mater. Chem. 11 (2001) 1408−1416.
[14] H. Assaaoudi, Z. Fang, D. Ryan, I.S. Butler, J.A. Kozinski, Can. J. Chem. 84 (2006) 124−133.
[15] J.M. Thomas, R. Raja, G. Sankar, R.G. Bell, Nature (London) 398 (1999) 227−230.
[16] J. Chen, J.M. Thomas, J. Chem. Soc. Chem. Commun. 5 (1994) 603−604.
[17] A.H. Shen, W.A. Bassett, I. Chou, Am. Mineral. 78 (1993) 694−698.
[18] G.M. Sheldrick, SHELXS97, Program for Crystal Structure Solution, University of Göttingen, Germany, 1997.
[19] G.M. Sheldrick, SHELXL97, Program for Crystal Structure Refinement, University of Göttingen, Germany, 1997.
[20] M.N. Burnett, C.K. Johnson, ORTEP-III, Oak Ridge National Laboratory Report ORNL-6895, 1996.
[21] L.J. Farrugia, ORTEP-3 for Windows − a version of ORTEP-III with a graphical user interface (GUI), J. Appl. Crystallogr. 30 (1997) 565.
[22] L. Popovic, D. de Waal, J.C.A. Boeyens, J. Raman Spectrosc. 36 (2005) 2−11.
[23] S. Krimi, A. El Jazouli, L. Rabardel, M. Couzi, I. Mansouri, G. Le Flem, J. Solid State Chem. 102 (1993) 400−407.
[24] H. Assaaoudi, I.S. Butler, J.A. Kozinski, F. Bélanger-Gariépy, J. Chem. Crystallogr. 35 (10) (2005) 809−820.
[25] (a) M. Harcharras, A. Ennaciri, H. Assaaoudi, Can. J. Anal. Sci. Spectros. 46 (3) (2001) 83−88;
(b) M. Harcharras, A. Ennaciri, A. Rulmont, B. Gilbert, Spectrochim. Acta A53 (1997) 345−352.

Fig. 8. Raman spectra of (a) amorphous powder obtained after reaction at SCW and (b) the material obtained after heating at 800 °C.

[26] O. Sarr, L. Diop, Spectrochim. Acta A40 (1984) 1011–1015.
[27] (a) Y. Hikichi, Phosphorus Lett. 41 (2001) 16–24;
(b) Y. Hikichi, T. Ota, K. Daimon, T. Hattori, M. Mizuno, J. Am. Ceram. Soc. 81 (8) (1998) 2216–2218.
[28] C.E. Bamberger, E.D. Specht, L.M. Anovitz, J. Am. Ceram. Soc. 80 (12) (1997) 3133–3138.
[29] V. Ramakrishnan, G. Aruldhas, Infrared Phys. Technol. 28 (2) (1988) 77–81.
[30] M. Baril, H. Assaaoudi, I.S. Butler, J. Mol. Struct. 751 (2005) 168–171.
[31] G. Herzberg, Infrared and Raman Spectra of Polyatomic Molecules, Van Nostrand, Princeton, New Jersey, 1946.
[32] R.S. Halford, J. Chem. Phys. 14 (1946) 8–15.